Biochemical and Structural Characterization of a Novel Class of Inhibitors of the Type 1 Insulin-like Growth Factor and Insulin Receptor Kinases

Ian M. Bell,*,‡ Steven M. Stirdivant,*,§ Janet Ahern,§ J. Christopher Culberson,|| Paul L. Darke,⊥ Christopher J. Dinsmore,‡ Robert A. Drakas,§ Steven N. Gallicchio,‡ Samuel L. Graham,‡ David C. Heimbrook,§ Dawn L. Hall,⊥ Jin Hua,§ Nathan R. Kett,‡ Annette S. Kim,‡ Maria Kornienko,⊥ Lawrence C. Kuo,⊥ Sanjeev K. Munshi,⊥ Amy G. Quigley,‡ John C. Reid,⊥ B. Wesley Trotter,‡ Lloyd H. Waxman,⊥ Theresa M. Williams,‡ and C. Blair Zartman‡

Departments of Cancer Research, Medicinal Chemistry, Molecular Systems, and Structural Biology, Merck Research Laboratories, West Point, Pennsylvania 19486

Received January 12, 2005; Revised Manuscript Received May 11, 2005

ABSTRACT: The type 1 insulin-like growth factor receptor (IGF-1R) is often overexpressed on tumor cells and is believed to play an important role in anchorage-independent proliferation. Additionally, cell culture studies have indicated that IGF-1R confers increased resistance to apoptosis caused by radiation or chemotherapeutic agents. Thus, inhibitors of the intracellular kinase domain of this receptor may have utility for the clinical treatment of cancer. As part of an effort to develop clinically useful inhibitors of IGF-1R kinase, a novel class of pyrrole-5-carboxaldehyde compounds was investigated. The compounds exhibited selectivity against the closely related insulin receptor kinase intrinsically and in cell-based assays. The inhibitors formed a reversible, covalent adduct at the kinase active site, and treatment of such adducts with sodium borohydride irreversibly inactivated the enzyme. Analysis of a tryptic digest of a covalently modified IGF-1R kinase fragment revealed that the active site Lys1003 had been reductively alkylated with the aldehyde inhibitor. Reductive alkylation of the insulin receptor kinase with one of these inhibitors led to a similarly inactivated enzyme which was examined by X-ray crystallography. The crystal structure confirmed the modification of the active site lysine side chain and revealed details of the key interactions between the inhibitor and enzyme.

Malignant neoplasms are characterized by multiple defects, including the loss of proliferative stop signals, decreased growth factor dependence, sustained proliferation, evasion of apoptosis, angiogenesis, motility, and invasiveness (*1*). It is now recognized that signaling from receptor tyrosine kinases (RTKs) is often unregulated in human cancers and that such activated RTKs can contribute to many of the tumor phenotypes that have been described (*2*, *3*). Identification of the roles of RTKs in cancer initiation and progression has resulted in drug discovery efforts aimed at their inhibition. Herceptin and Iressa, directed against Her2 and EGFR, respectively, are two examples of agents which have demonstrated clinical utility (*4*, *5*). More recently, the RTK insulin-like growth factor receptor (IGF-1R) has attracted considerable attention as a potential antineoplastic target (*6*−*8*). Laboratory studies have demonstrated the role of the IGF axis in cell proliferation, transformation, survival signaling, angiogenesis, invasion, and metastasis (*8*, *9*). IGF-1R may contribute to chemoresistance in cancer cells through its antiapoptotic function (*10*−*14*). Moreover, clinical observations have indicated that the IGF axis may play a role in cancer risk, progression, disease stage, and prognosis (*15*−*26*).

The IGF axis consists of IGF-1R, its ligands (IGF-1 and IGF-2), and a set of six IGFBPs[1] which serve to modulate the effective serum concentration of IGF-1 (*9*). IGF-1R is composed of two extracellular α subunits and two β subunits having extracellular, transmembrane, and intracellular domains. It is thought that binding of ligand to the α subunits causes a conformational change in the receptor, leading to trans-autophosphorylation of tyrosine residues in the β subunits, both within the intracellular kinase domain and outside the catalytic domain (*9*, *27*). While autophosphorylation of the activation loop within the kinase active site enhances catalytic activity (*28*), the phosphotyrosines outside the kinase domain serve as docking sites for proteins that contain phosphotyrosine binding motifs (*9*, *29*). Proteins which dock to IGF-1R, such as IRS-1, Grb2, or Shc, serve to initiate downstream signaling pathways, of which the MAPK and Akt (PKB) pathways appear to play a dominant

* To whom correspondence should be addressed. I.M.B.: telephone, (215) 652-6455; fax, (215) 652-7310; e-mail, ian_bell@merck.com. S.M.S.: telephone, (215) 652-3337; e-mail, steven_stirdivant@merck.com.
‡ Department of Medicinal Chemistry.
§ Department of Cancer Research.
|| Department of Molecular Systems.
⊥ Department of Structural Biology.

[1] Abbreviations: AcOH, acetic acid; BSA, bovine serum albumin; DMF, *N*,*N*-dimethylformamide; DTT, dithiothreitol; EDC, 1-(3-dimethylaminopropyl)-3-ethylcarbodiimide hydrochloride; EDTA, ethylenediaminetetraacetic acid; GST, glutathione *S*-transferase; HEPES, 4-(2-hydroxyethyl)-1-piperazineethanesulfonic acid; HOBT, 1-hydroxybenzotriazole hydrate; IGFBP, IGF binding protein; TFA, trifluoroacetic acid; THF, tetrahydrofuran; Tris, tris(hydroxymethyl)aminomethane.

10.1021/bi0500628 CCC: $30.25
Published on Web 06/17/2005

role in mediating IGF-1R function (*29*−*31*). Mutants of IGF-1R lacking kinase activity fail to activate these downstream signaling pathways and do not facilitate the phenotypes associated with the IGF axis (*32*−*34*).

The role of IGF-1R in tumorigenesis and resistance to chemotherapeutic agents suggests that it may be a viable therapeutic target, and drug discovery efforts employing both small molecule (*35*, *36*) and antibody (*37*) approaches have been reported. One challenge for small molecule kinase inhibitor development is the high degree of homology (84%) between the IGF-1R and IR kinase domains. Even more daunting is the 100% identity among amino acid residues within the immediate ATP binding pocket (*38*).

Here, we describe a class of small molecule IGF-1R inhibitors with a novel binding mechanism. These pyrrole-5-carboxaldehyde inhibitors are ATP competitive, and form a reversible, covalent adduct between the aldehyde moiety and a lysine residue within the IGF-1R ATP binding pocket. The compounds show a degree of selectivity for inhibition of IGF-1R over IR in multiple assays, including a cell-based autophosphorylation assay.

MATERIALS AND METHODS

General Chemical Methods. Proton NMR spectra were recorded at 500 MHz on Varian spectrometers, and chemical shifts are reported in parts per million (δ) downfield from tetramethylsilane as the internal standard. Electrospray mass spectra were recorded on a Micromass ZMD spectrometer. Analytical thin-layer chromatography was conducted with EM Science Kieselgel 60 F_{254} plates. Silica gel chromatography was performed with an ISCO Combiflash Sg 100c instrument using prepacked RediSep or Biotage silica cartridges. A Hewlett-Packard 1100 Series HPLC system with a MetaChem Inertsil column was used for analytical HPLC, eluting with a gradient from H_2O and 0.1% TFA to CH_3CN and 0.08% TFA (from 95:5 to 0:100 over the course of 5 min). Reagents and solvents were obtained from commercial sources and used without further purification. The reported yields are the actual isolated yields of purified material and are not optimized.

Known compounds **1** (*39*), **2** (*40*), and **3** (*41*) were synthesized using a methodology analogous to that used for compounds **5** and **6** (vide infra). The kinase inhibitor **K252a** was purchased from Calbiochem.

*N,N,N′,N′-Tetraethyl-5-formyl-3-methyl-1H-pyrrole-2,4-dicarboxamide (**4**).* Using a methodology analogous to that used for compounds **5** and **6**, the title compound was obtained (12 mg, 29%): ^{1}H NMR (CD_3OD) δ 9.49 (1H, s), 3.70−3.28 (8H, m), 2.00 (3H, s), 1.30−1.04 (12H, m); MS (ES) *m*/*z* 308 (MH^+); HRMS (FAB) *m*/*z* for MH^+ ($C_{16}H_{26}N_3O_3$) calcd 308.1969, found 308.1995; HPLC purity 100% (215 nm).

*2-tert-Butyl 4-Ethyl 3-Ethyl-5-formyl-1H-pyrrole-2,4-dicarboxylate (**5**). 2-tert-Butyl 4-Ethyl 3-Ethyl-5-methyl-1H-pyrrole-2,4-dicarboxylate*. To a stirred solution of *tert*-butyl 3-oxopentanoate (*42*) (1.39 g, 8.07 mmol) in AcOH (5 mL), at 0 °C, was added dropwise a solution of $NaNO_2$ (0.53 g, 7.68 mmol) in H_2O (1.5 mL). The mixture was allowed to warm to ambient temperature, and stirring was continued for 2 h. The resulting mixture was added dropwise to a stirred mixture of ethyl acetoacetate (1.16 g, 8.91 mmol), zinc powder (1.66 g, 25.4 mmol), and ammonium acetate (1.56 g, 20.2 mmol) in AcOH (5 mL). After the addition, the reaction temperature increased to 75 °C over the course of 10 min. The mixture was stirred for 5 h, quenched with H_2O (100 mL), and extracted with CH_2Cl_2 (3 × 100 mL). The combined organic extracts were washed with saturated aqueous $NaHCO_3$ (100 mL), dried over Na_2SO_4, filtered, and concentrated in vacuo to give a crude solid. The crude product was purified by silica gel chromatography, eluting with a hexane/EtOAc gradient (from 100:0 to 80:20) to give the title compound as a pale solid (0.90 g, 40%): ^{1}H NMR ($CDCl_3$) δ 8.84 (1H, br s), 4.29 (2H, q, J = 7.1 Hz), 3.05 (2H, q, J = 7.3 Hz), 2.50 (3H, s), 1.57 (9H, s), 1.36 (3H, t, J = 7.1 Hz), 1.16 (3H, t, J = 7.3 Hz); MS (ES) *m*/*z* 282 (MH^+); HPLC purity 95% (215 nm).

*2-tert-Butyl 4-Ethyl 3-Ethyl-5-formyl-1H-pyrrole-2,4-dicarboxylate (**5**).* To a stirred solution of 2-*tert*-butyl 4-ethyl 3-ethyl-5-methyl-1*H*-pyrrole-2,4-dicarboxylate (212 mg, 0.75 mmol) in THF (4 mL), H_2O (4 mL), and AcOH (4.8 mL) was added ceric ammonium nitrate (824 mg, 1.50 mmol), and the mixture was stirred at ambient temperature for 2 h. Saturated aqueous Na_2CO_3 (50 mL) was added carefully to basify the reaction mixture, followed by extraction with CH_2Cl_2 (3 × 40 mL). The combined organic extracts were dried over Na_2SO_4, filtered, and concentrated in vacuo to give a crude product, which was purified by silica gel chromatography, eluting with a hexane/EtOAc gradient (from 95:5 to 80:20) to give the title compound as a pale solid (44 mg, 20%): ^{1}H NMR ($CDCl_3$) δ 10.25 (1H, s), 9.85 (1H, br s), 4.40 (2H, q, J = 7.2 Hz), 3.09 (2H, q, J = 7.4 Hz), 1.60 (9H, s), 1.41 (3H, t, J = 7.2 Hz), 1.19 (3H, t, J = 7.4 Hz); MS (ES) *m*/*z* 296 (MH^+); HRMS (FAB) *m*/*z* for MH^+ ($C_{15}H_{22}NO_5$) calcd 296.1493, found 296.1515; HPLC purity 99% (215 nm).

*Ethyl 5-[(tert-Butylamino)carbonyl]-4-ethyl-2-formyl-1H-pyrrole-3-carboxylate (**6**). 4-(Ethoxycarbonyl)-3-ethyl-5-methyl-1H-pyrrole-2-carboxylic Acid.* To a stirred solution of 2-*tert*-butyl 4-ethyl 3-ethyl-5-methyl-1*H*-pyrrole-2,4-dicarboxylate (171 mg, 0.61 mmol) in AcOH (1.5 mL) was added 48% HBr (0.102 mL, 0.61 mmol), and the mixture was stirred for 6 h at ambient temperature. The mixture was cooled to 0 °C, and CH_2Cl_2 (10 mL) was added. The white precipitate was collected by filtration, and the filtrate was concentrated to dryness under reduced pressure. The residue was triturated with CH_2Cl_2 (10 mL) to give another crop of white solid. The combined solids were the title compound (106 mg, 77%): ^{1}H NMR (CD_3OD) δ 4.26 (2H, q, J = 7.1 Hz), 3.08 (2H, q, J = 7.3 Hz), 2.45 (3H, s), 1.35 (3H, t, J = 7.1 Hz), 1.12 (3H, t, J = 7.3 Hz); MS (ES) *m*/*z* 226 (MH^+); HPLC purity 95% (215 nm).

Ethyl 5-[(tert-Butylamino)carbonyl]-4-ethyl-2-methyl-1H-pyrrole-3-carboxylate. A mixture of 4-(ethoxycarbonyl)-3-ethyl-5-methyl-1*H*-pyrrole-2-carboxylic acid (37 mg, 0.16 mmol), *tert*-butylamine (42 mg, 0.57 mmol), HOBT (26 mg, 0.19 mmol), and EDC (40 mg, 0.21 mmol) in DMF (0.4 mL) was stirred for 3 h at ambient temperature. The mixture was purified by reverse-phase HPLC on a YMC Pack Pro C18 column, eluting with a H_2O/CH_3CN/TFA gradient (from 95:5:0.1 to 5:95:0.1). The pure product-containing fractions were combined, adjusted to pH 8 with saturated aqueous $NaHCO_3$, and extracted with CH_2Cl_2 (3 × 30 mL). The combined organic extracts were dried over Na_2SO_4, filtered,

and concentrated in vacuo to give the title compound as a white solid (28 mg, 61%): ^{1}H NMR ($CDCl_3$) δ 9.68 (1H, br s), 5.75 (1H, br s), 4.28 (2H, q, $J = 7.1$ Hz), 2.96 (2H, q, $J = 7.5$ Hz), 2.48 (3H, s), 1.46 (9H, s), 1.36 (3H, t, $J = 7.1$ Hz), 1.24 (3H, t, $J = 7.5$ Hz); MS (ES) *m*/*z* 281 (MH^+); HPLC purity 98% (215 nm).

*Ethyl 5-[(tert-Butylamino)carbonyl]-4-ethyl-2-formyl-1H-pyrrole-3-carboxylate (**6**).* Using the method described for compound **5**, ethyl 5-[(*tert*-butylamino)carbonyl]-4-ethyl-2-methyl-1*H*-pyrrole-3-carboxylate was oxidized to give the title compound (6 mg, 20%): ^{1}H NMR ($CDCl_3$) δ 10.21 (1H, s), 10.14 (1H, br s), 5.93 (1H, br s), 4.39 (2H, q, $J = 7.2$ Hz), 3.00 (2H, q, $J = 7.6$ Hz), 1.47 (9H, s), 1.41 (3H, t, $J = 7.2$ Hz), 1.27 (3H, t, $J = 7.4$ Hz); MS (ES) *m*/*z* 295 (MH^+); HRMS (FAB) *m*/*z* for MH^+ ($C_{15}H_{23}N_2O_4$) calcd 295.1653, found 295.1679; HPLC purity 97% (215 nm).

*2-tert-Butyl 4-Ethyl 3-Ethyl-5-formyl-1-methyl-1H-pyrrole-2,4-dicarboxylate (**7**).* To a suspension of 18-crown-6 (3.6 mg, 0.01 mmol) and potassium *tert*-butoxide (18.2 mg, 0.16 mmol) in Et_2O (1.5 mL) was added **6** (40 mg, 0.14 mmol) in one portion. The reaction mixture was stirred at ambient temperature for 15 min, and then MeI (0.010 mL, 0.16 mmol) was added. The resulting solution was stirred at ambient temperature for 18 h. The reaction mixture was diluted with EtOAc (20 mL) and washed with H_2O (3 × 10 mL). The EtOAc layer was then washed with brine (10 mL), and the combined aqueous layers were washed with EtOAc (20 mL). The combined organic layers were dried over $MgSO_4$, filtered, and concentrated in vacuo. The mixture was purified by reverse-phase HPLC on a YMC Pack Pro C18 column, eluting with a H_2O/CH_3CN/TFA gradient (from 95:5:0.1 to 5:95:0.1). The pure product-containing fractions were combined, adjusted to pH 8 with saturated aqueous $NaHCO_3$, and extracted with EtOAc (30 mL). The combined organic extracts were dried over Na_2SO_4, filtered, and concentrated in vacuo to give the title compound as a white solid (21 mg, 50%): ^{1}H NMR (500 MHz, $CDCl_3$) δ 10.35 (1H, s), 4.37 (2H, q, $J = 7.2$ Hz), 4.14 (1H, s), 2.93 (2H, q, $J = 7.3$ Hz), 1.6 (9H, s), 1.4 (3H, t, $J = 7.1$ Hz), 1.2 (3H, t, $J = 7.5$ Hz); MS (ES) *m*/*z* 295 (MH^+); HRMS (ES) *m*/*z* for MH^+ ($C_{16}H_{24}NO_5$) calcd 310.1649, found 310.1650.

Computational Chemistry. Calculated logP values (ClogP) were obtained using ACD/Labs 6.00 (Advanced Chemistry Development Inc.). In the molecular modeling studies described herein, energy minimization was carried out using the MMFF force field with Macromodel (*43*) to provide low-energy structures.

IGFRK and IRK Constructs. The intracellular kinase domains of human IGF-1R and human IR were cloned as GST fusion proteins beginning with the first juxtamembrane amino acid for each β subunit. IGF-1R β subunit amino acid residues 930−1337 [numbering system of Ullrich et al. (*38*)] were cloned into the baculovirus transfer vector pAcGHLT-A (BD-Pharmingen) such that the N-terminus of the IGF-1R sequence was fused to the C-terminus of the GST domain encoded in the transfer vector. IR β subunit residues 941−1343 [numbering system of Ullrich et al. (*44*)] were cloned into pAcGHLT-A in a similar fashion. Recombinant viruses were generated and the fusion proteins expressed in SF-9 insect cells (BD-Pharmingen). Enzymes were purified using a glutathione-Sepharose column. The IGFRK306 form of the IGF-1R β subunit was constructed using standard PCR methodology and contains IGF-1R amino acids 951−1256 with an N-terminal methionine and no GST tag. In addition, tyrosines 957, 1250, and 1251 of IGFRK306 were substituted with phenylalanines by sequence manipulation of the N- and C-terminal PCR primers used to amplify the IGFRK306 coding sequence. The resulting IGFRK306 construct was expressed in SF-9 insect cells and purified by conventional chromatography methods.

IGFRK and IRK Assays. The kinase assays using IGF-1R and IR kinase GST fusion proteins were conducted using a homogeneous time-resolved fluorescence (HTRF) format. The assays were performed in a manner similar to the manner used for the assays described by Park et al. (*45*). Briefly, the kinase reactions were carried out in a 96-well plate format in a final volume of 60 μL. The standard enzyme reaction buffer consisted of 50 mM Tris-HCl (pH 7.4), 100 mM NaCl, 5 mM $MgCl_2$, 2 mM DTT, 0.1% BSA, 2 mM ATP, 0.1 μM peptide substrate (biotin-EQEDEPEGDYFEWLE-NH_2), and 0.1 nM GST−IGFRK or GST−IRK fusion protein. Inhibitor, in DMSO (1 μL), was added to give a final inhibitor concentration ranging from 1 nM to 100 μM, and the mixture was preincubated for 10 min at 22 °C. The kinase reaction was initiated with 40 mM ATP (3 μL). After 20 min at 22 °C, the reaction was stopped with 40 μL of quench buffer [125 mM Tris-HCl (pH 7.8), 75 mM EDTA, 0.5 M KF, 0.125% Triton X-100, 1.25% BSA, 150 nM SA-XL665 (Packard), and 0.75 nM europium cryptate-labeled anti-phosphotyrosine antibody (PY20, Santa Cruz Biotechnology)] and the mixture allowed to equilibrate for 2 h at 22 °C. Relative fluorescence units were read on a Discovery plate reader (Packard). The IC_{50} values for inhibitors were determined by a four-parameter sigmoidal curve fit.

Other Kinase Assays. For kinase counter-screening, PKC-α, p70S6K, casein kinase 2, and Chek2 were purchased from Upstate Cell Signaling Solutions and assayed in a [^{33}P]ATP filter binding format at 100 μM ATP using the manufacturer's protocol. AMPK (Upstate) and MARK3 (Upstate) were assayed at 100 μM ATP in an HTRF format similar to that employed for IGFRK (vide supra) but utilizing a biotinylated peptide substrate (biotin-GGRARTSSFAEPS-OH) and a europium chelate (Perkin-Elmer)-conjugated anti-phospho GSK3α antibody (Cell Signaling Technologies). EGFR (Promega), c-Src (Upstate), c-Abl (Calbiochem), and KDR (*46*) were assayed at 2 mM ATP using the same assay conditions and peptide substrate that were used for IGFRK (vide supra).

Enzyme Autophosphorylation Assay. Transphosphorylation of the receptor β subunit was assessed in a HTRF-based assay using the GST−IGF-1R and GST−IR fusion proteins. Assays were carried out at 23 °C under conditions used in the peptide substrate assays (vide supra) but with either fusion protein at 2 nM and no exogenous peptide substrate. Reaction mixtures were assembled in a volume of 0.9 mL, for each inhibitor concentration. A 100× concentration of inhibitor was added to each reaction mixture, and the mixture was allowed to equilibrate for 15 min. Reactions were initiated with the addition of ATP (final concentration of 2 mM). At the required time points, 50 μL aliquots of the reaction mixtures were removed and the reactions stopped in 50 μL of quench buffer (vide supra) containing 2 nM europium chelate-conjugated PY20 antibody (Perkin-Elmer) and either 12.8 nM allophycocyanin-conjugated anti-IGF-1R β subunit

antibody for IGFRK [SC-713 antibody (Santa Cruz), conjugated using the phycolink allophycocyanin conjugation kit (Prozyme PJ25K)] or allophycocyanin-conjugated anti-IR β subunit antibody for IRK [SC-711 antibody (Santa Cruz), conjugated using the phycolink allophycocyanin conjugation kit (Prozyme PJ25K)]. Standard receptor phosphorylation curves were developed by mixing fully phosphorylated GST−IGF-1R or GST−IR with varying proportions of the nonphosphorylated receptors at a concentration of 2 nM in reaction buffer without ATP. The extent of receptor phosphorylation was quantitated in the Discovery plate reader, relating the fluorescence signal to receptor phosphorylation through the standard curve. Reaction progress curves were generated, and an apparent rate was calculated by fitting the exponential rise to maximum curves to the equation $y = a(1 - e^{-bt})$, where a is the maximal phosphorylation signal and b is the rate. The IC_{50} values for the test compounds were obtained from plots of calculated rates versus inhibitor concentration.

$NaBH_4$ Reductions. A 0.5 M stock of $NaBH_4$ was prepared in 0.5 M Tris-HCl (pH 7.4). The test compound and GST kinase (final concentration of 3 nM) were preincubated in 120 mM Tris-HCl (pH 7.4), 100 mM NaCl, 5 mM $MgCl_2$, 2 mM DTT, and 0.1% BSA for 15 min at ambient temperature. The 0.5 M $NaBH_4$ solution (0.22 mL) was added (50 mM final), and the reaction was allowed to proceed at ambient temperature for 20 min. $NaBH_4$ and unbound inhibitor were removed by passing 2.0 mL of the reaction mixture through a PD10 column equilibrated with enzyme reaction buffer (without substrate peptide and ATP). Enzyme was eluted from the column with the addition of 3.5 mL of the same buffer. The remaining enzyme activity was assayed in the HTRF format by adding 0.1 μM peptide substrate and 2 mM ATP to the eluted enzyme in reaction buffer.

HEK-IGF-1R and HEK-IR Cell Lines. Human embryonic kidney cells (HEK-293) (ATCC) were transfected with an expression plasmid containing the entire IGF-1R or IR coding sequence (expression plasmids were a gift from B. Zhang, Merck). After antibiotic selection, colonies were screened for IGF-1R or IR overexpression by Western blot analysis. Strongly expressing clones were selected for cell-based autophosphorylation assays.

Cell-Based Autophosphorylation Assay. HEK cells overexpressing IGF-1R (or IR) were seeded in MEM with 0.5% fetal bovine serum at 8×10^4 cells per well in a 96-well fibronectin-coated plate (Becton-Dickinson) and allowed to adhere overnight. A 10× concentration of compound diluted in medium was added to the wells and incubated for 2 h, at which time IGF-1 (or insulin) was added to a final concentration of 20 μM. After a 10 min incubation, the medium was aspirated off and 80 μL of lysis buffer [50 mM HEPES (pH 7.6), 150 mM NaCl, 1 mM EDTA, 10% glycerol, 1% Triton X-100, 10 mM NaF, 0.5 mM Na_3VO_4, and 1× protease inhibitor cocktail (Boehringer)] was added to the wells. Plates were shaken for 1 h, and 60 μL of lysate was removed and transferred to a black 96-well plate (Thermal Lab Systems); 60 μL of quench buffer [500 mM KF, 125 mM Tris (pH 8), 75 mM EDTA, 1.25% BSA, and 0.125% Triton X-100] containing 2.5 nM APC-conjugated SC-713 antibody (or SC-711 antibody) and 4 nM Eu-PY20 antibody was added, bringing the total volume to 120 μL. Plates were shaken overnight at 4 °C and analyzed in a Discovery fluorescence plate reader (Packard).

Protein Digestion and Analysis. IGFRK306 (80 μg in 100 μL), covalently modified by treatment with **1** and $NaBH_4$, was precipitated by the addition of an equal volume of 20% (w/v) trichloroacetic acid and left overnight at 4 °C. The precipitated protein was collected by centrifugation, and the precipitate was washed three times with methanol (500 μL) to remove traces of trichloroacetic acid and resuspended in 50 mM ammonium bicarbonate. Porcine trypsin (1 μg, Promega) was added, and digestion was carried out for 8 h at 25 °C. The mixture was taken to near dryness in a SpeedVac, and the peptides were dissolved in 1% acetic acid (100 μL). An unmodified sample of IGFRK306 was treated similarly.

The digests were analyzed by reverse-phase HPLC on a Vydac 2.1 mm × 150 mm C18 column using a Waters HPLC system. The peptides were fractionated by means of a linear gradient of CH_3CN in 0.06% TFA from 0 to 50% over the course of 60 min and from 50 to 98% over the course of 30 min at a flow rate of 1 mL/min.

Analysis of proteins and peptides by liquid chromatography and mass spectrometry (LC−MS) was carried out on an Agilent model 1100 HPLC system in series with a Thermo Finnigan LCQ Deca mass spectrometer equipped with an electrospray source. Samples were injected onto a Jupiter C4 or Vydac C18 column (2.1 mm × 150 mm) and eluted using a gradient of CH_3CN in 0.1% AcOH and 0.02% TFA at a flow rate of 0.2 mL/min. The electrospray data were deconvoluted to obtain polypeptide masses using Xcalibur software. Theoretical masses were calculated using the ProteinProspector program available on-line (*47*).

*Crystallization of the Complex of the IR Kinase Domain and Compound **5***. The tyrosine kinase domain of IR was cloned and expressed in the baculovirus system and purified as described previously (*48*). Crystals for the covalent complex of compound **5** and the tyrosine kinase domain of IR were obtained by vapor diffusion using hanging drops incubated at 4 °C. Crystals were obtained by mixing the protein solution and reservoir buffer (1:1 by volume). The reservoir solution consisted of 18% polyethylene glycol 8000, 0.1 M Tris-HCl (pH 7.5), and 2% ethylene glycol. The protein−inhibitor complex at 15 mg/mL was suspended in a solution consisting of 20 mM Tris-HCl (pH 7.5) and 5 mM DTT. Plate-shaped crystals appeared in 3 days and grew to full size of ∼0.1 mm × 0.1 mm × 0.1 mm.

Data Collection and Structure Determination. Crystals were harvested into a solution containing the reservoir buffer and 20% glycerol. The crystals were left sitting for 5 min and subsequently transferred onto the goniostat, which was bathed in a nitrogen stream cooled to −180 °C. X-ray diffraction data were recorded using the RAXIS-II imaging plate system and RU300 X-ray generator operating at 50 kV and 100 mA. The crystals belonged to space group $P2_12_12_1$ with one kinase molecule in the asymmetric unit. The data were processed using HKL2000 (*49*). Diffraction data and refinement statistics are given in Table 4.

The structure of the kinase domain of IR covalently bound to compound **5** was determined by molecular replacement using AMoRe (*50*, *51*). The structure of the unactivated IR kinase domain (*52*) was used as the phasing model. Model building was carried out using the X-BUILD option in

Table 1: Activity of Pyrrole Analogues as Inhibitors of IGFRK and IRK

compound	IGFRK IC_{50} (μM)	IRK IC_{50} (μM)	IGF-1R cell autophosphorylation IC_{50} (μM)
1	2.7 ± 0.90	12 ± 5.4	15
2	1.1 ± 0.57	5.4 ± 2.4	2.9 ± 0.97
3	>100	>100	>100
4	>100	>100	>100
5	0.49 ± 0.15	2.0 ± 0.45	5.3 ± 0.8
6	2.6 ± 1.0	17 ± 6.5	8.2 ± 2.3
7	4.3 ± 1.6	12 ± 5.2	–
K252a	0.47 ± 0.15	0.21 ± 0.05	–

Table 2: Inhibition of Kinase Enzymes by Compound **1**

kinase	IC_{50} (μM)	% inhibition at 100 μM **1**
IGF-1R	2.7 ± 0.90	100
IR	12 ± 5.4	93
p70S6K	>100	45
Chek2	>100	24
AMPK	>100	20
EGFR	>100	0
c-Abl	>100	0
c-Src	>100	0
KDR	>100	0
MARK3 (c-Tak)	>100	0
casein kinase 2	>100	0
PKC-α	>100	0

program suite QUANTA, and refinement was carried using CNX (Molecular Simulations Inc., San Diego, CA) (*53*).

RESULTS AND DISCUSSION

Enzyme Assays. The standard kinase assays for IGF-1R and IR were run in a coupled format at 2 mM ATP (Table 1). Prior to initiation of the reactions with ATP, the kinases were in a nonphosphorylated, unactivated form. Upon addition of ATP, autophosphorylation of the kinase activation loop occurred, activating kinase activity toward the tyrosine-containing peptide substrate. The HTRF detection system assessed phosphorylation of the peptide substrate. Therefore, the "coupled" assay detected inhibition of the autophosphorylation event (indirectly) as well as inhibition of phosphorylation of the peptide substrate by the activated enzyme. The two activities represented in the coupled assay were also measured independently. The autophosphorylation reaction of kinase domain tyrosines was quantitated directly in the HTRF-based enzyme autophosphorylation assay, while inhibition of the activated enzyme was assessed by employing a preactivated kinase and initiating the reaction with peptide substrate. While the coupled assay allowed an assessment of overall kinase inhibition, the autophosphorylation and preactivated assays permitted an analysis of the interaction of inhibitors with the two different conformational forms of the kinase (Table 3).

Structure–Activity Relationships of Pyrrole-Based Inhibitors. Screening lead **1** (Chart 1) was a moderately potent, low-molecular weight, cell active lead, which was competitive versus ATP when titrated against activated IGFRK (see Table 1 and Figure 1). The most attractive feature of **1** was its apparent selectivity for IGFRK over IRK which, although modest, was not an artifact of these assays but was a property of the compounds, since the unrelated kinase inhibitor **K252a** was selective for IRK over IGFRK (Table 1). Furthermore, compound **1** was tested against a panel of other kinases and was not a significant inhibitor (IC_{50} > 100 μM) of any of them (see Table 2). A chemistry effort was initiated with the goals of defining basic structure–activity relationships and determining whether the potency of the lead could be improved while maintaining selectivity against IRK.

Replacement of the 3-methyl substituent with an ethyl group gave **2**, which was ~2-fold more potent than **1** as an inhibitor of IGFRK (see Table 1). The enhanced intrinsic potency of **2** translated into the cell-based assay, and the compound maintained selectivity against IRK. Modification of the 2-position ethyl ester in **2** to give a *tert*-butyl ester (compound **5**) provided a small increase in intrinsic potency, while the corresponding *tert*-butyl amide (compound **6**) was less potent. Taken together, these observations suggested that the substituents at the 2- and 3-positions on the pyrrole were

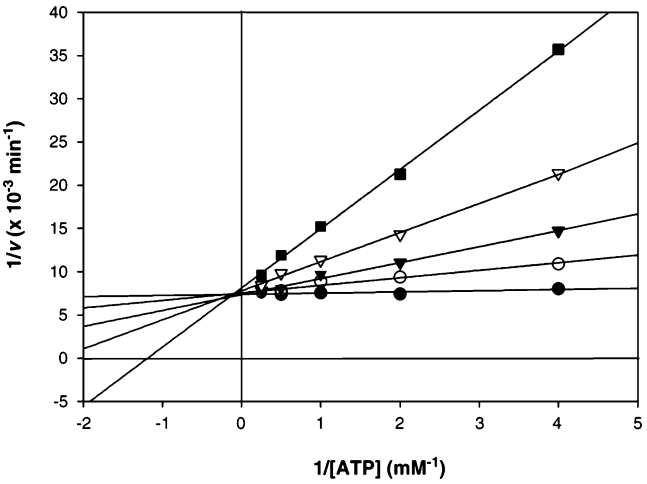

FIGURE 1: Lineweaver–Burk plot of $1/v$ vs 1/[ATP] for the activated form of IGFRK at **1** concentrations of 0 (●), 25 (○), 50 (▼), 100 (▽), and 200 μM (■). Velocity (v) is defined as [$\Delta(f_{665}/f_{615})$]/min, measured over a linear range of the reaction.

Chart 1: Structures of Pyrrole Analogues

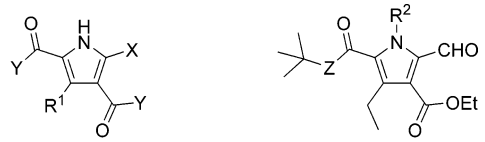

1 (R^1 = Me, X = CHO, Y = OEt)
2 (R^1 = Et, X = CHO, Y = OEt)
3 (R^1 = Me, X = CH_2OH, Y = OEt)
4 (R^1 = Me, X = CHO, Y = NEt_2)

5 (R^2 = H, Z = O)
6 (R^2 = H, Z = NH)
7 (R^2 = Me, Z = O)

Table 3: IC_{50} Values (μM) for Selected Pyrrole Analogues as Inhibitors of IGFRK and IRK

compound	IGFRK, coupled[a]	IGFRK, autophosphorylation[a]	IGFRK, activated[b]	IRK, coupled[a]	IRK, autophosphorylation[a]	IRK, activated[b]	IRK:IGFRK ratio, autophosphorylation	IRK:IGFRK ratio, activated
2	1.1	0.23	40	5.4	1.4	80	6.1	2.0
5	0.49	0.11	17	2	0.6	40	5.5	2.4
6	2.6	0.58	100	17	3.3	210	5.7	2.1

[a] Assay carried out with 2 mM ATP. [b] Assay carried out with 0.1 mM ATP.

Table 4: Structure Determination and Refinement

space group	$P2_12_12_1$
unit cell constants	$a = 54.5$ Å, $b = 73.7$ Å, $c = 90.3$ Å, $\alpha = 90°$, $\beta = 90°$, $\gamma = 90°$
resolution (Å)	2.0
no. of observed reflections	284051
no. of unique reflections	24445
completeness (%)	96.5 (95.5)
R_{sym} (%)	5.3 (20.6)
$I/\sigma(I)$	20 (5.5)
refinement resolution limits (Å)	8−2.0
R_{work} (%)	25.3
R_{free} (%)	28.7

interacting with a hydrophobic part of the active site. They also demonstrated that it was possible to increase the inhibitory potency of the compounds without reducing selectivity against IRK. Notably, the ratio of IGFRK and IRK IC_{50} values was similar for all active pyrrolecarboxaldehyde compounds in Table 1, indicating that the modifications that were made affected the ability of the analogues to bind to each active site to a similar extent. This was not surprising given the high degree of homology between the two kinase domains. Interestingly, the activity of **5** and **6** in cells was similar despite their different intrinsic potencies, perhaps because the cell permeability of **5** was compromised by its higher lipophilicity. Calculated logP values support this possibility. For **5**, ClogP = 4.2; for **6**, ClogP = 3.3.

Inhibitors Preferentially Inhibited the Unactivated Forms of IGFRK and IRK. Three inhibitors were analyzed further for their activity against the unactivated and activated forms of IGFRK and IRK. Figure 2 shows a representative autophosphorylation assay in which compound **2** was titrated against unactivated IGFRK and IRK. These pyrrole-based inhibitors were considerably more potent in the enzyme autophosphorylation assay than the preactivated enzyme assay (see Table 3). In fact, because of the decreased potency of the inhibitors against the activated forms of the kinases, the preactivated enzyme assays were run at a lower concentration of ATP (0.1 mM instead of 2 mM) to generate complete titration curves. Since [ATP] $\approx K_m$ in both the unactivated and preactivated enzyme assays,[2] the relative IC_{50} values should reflect the relative K_i values for binding of the inhibitor to the two enzyme forms. Therefore, these inhibitors had approximately 100-fold higher affinity for the unactivated enzyme compared with the activated enzyme, based on their IC_{50} values (see Table 3). Inhibition in the coupled assay was dominated by the compound's inhibition of autophosphorylation. The higher IC_{50} values obtained in the coupled assay relative to the autophosphorylation assay presumably reflected the contribution of the activated form of the enzyme. Gratifyingly, the relative potencies of the three compounds in Table 3 remained constant within the autophosphorylation assay and the preactivated assay.

The Inhibitors Possessed Greater IRK versus IGFRK Selectivity with the Unactivated Kinases. A comparison of the IRK:IGFRK IC_{50} ratios for the autophosphorylation and preactivated enzyme assays (Table 3) revealed a greater selectivity for inhibition of the unactivated form of the enzymes. This suggested that there were greater relative differences in the conformational states of the IGFRK and IRK ATP binding pockets when the kinases were in their unactivated states. Consistent with the modest IRK versus IGFRK selectivity seen in the enzyme autophosphorylation assays, compound **2** exhibited selectivity in inhibiting receptor autophosphorylation in the cell-based ligand-induced autophosphorylation assay (Figure 3; IGF-1R $IC_{50} = 2.9\ \mu$M,

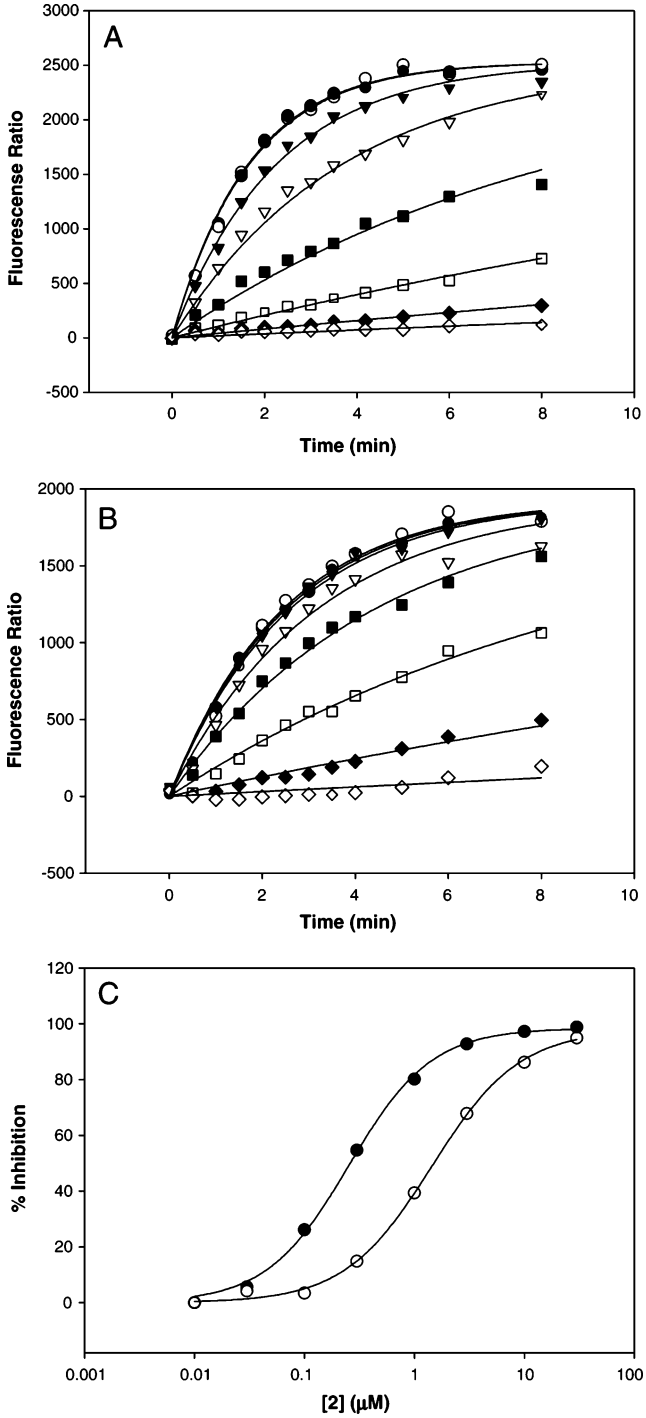

FIGURE 2: Enzyme autophosphorylation assays for inhibition of IGFRK and IRK by compound **2**. (A) Autophosphorylation time course for IGFRK at **2** concentrations of 0 (●), 0.03 (○), 0.1 (▼), 0.3 (▽), 1 (■), 3 (□), 10 (◆), and 30 μM (◇). (B) Autophosphorylation time course for IRK at **2** concentrations identical to those used for panel A. (C) Inhibition of autophosphorylation at varying **2** concentrations for IGFRK (●) and IRK (○). For compound **2**, IGFRK $IC_{50} = 0.26\ \mu$M and IRK $IC_{50} = 1.4\ \mu$M.

[2] The ATP K_m values for IGFRK were determined to be 2 mM (unactivated) and 0.1 mM (activated). The ATP K_m values for IRK were determined to be 1.5 mM (unactivated) and 0.07 mM (activated), in good agreement with previously reported data (*28*).

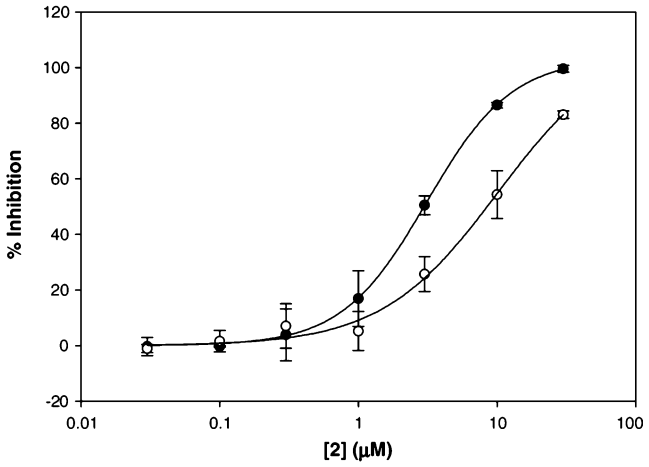

FIGURE 3: Inhibition of cell autophosphorylation at varying **2** concentrations for IGF-1R (●) and IR (○) overexpressed in HEK cells. For compound **2**, IGF-1R $IC_{50} = 2.9\ \mu M$ and IR $IC_{50} = 10.1\ \mu M$.

IR $IC_{50} = 10.1\ \mu M$, and IR:IGF-1R ratio = 3.5). In cell autophosphorylation assays, compound **5** (IGF-1R $IC_{50} = 5.3\ \mu M$; IR $IC_{50} = 22\ \mu M$) and compound **6** (IGF-1R $IC_{50} = 8.2\ \mu M$; IR $IC_{50} = 30\ \mu M$) were also 3−4-fold selective for IGF-1R over IR, indicating that selectivity observed in the GST fusion enzyme assays is reproduced when titrating autophosphorylation of the holo receptor in the cell membrane. While the modest cell potency of these analogues precluded in vivo studies, the consistent IRK versus IGFRK selectivity between in vitro enzyme and cellular inhibition assays differentiated these pyrroles from some other IGFRK inhibitors. For example, the pyrrolo[2,3-*d*]pyrimidine **NVP-AEW541** exhibited highly selective inhibition of IGF-1R autophosphorylation in cells (IR:IGF-1R ratio = 27) but no intrinsic selectivity in an enzyme inhibition assay (*35*).

Structure−Activity Relationships: Inactive Analogues. Table 1 details three modifications of these pyrrolecarboxaldehyde inhibitors that were poorly tolerated. Methylation of the pyrrole nitrogen led to a 9-fold loss in potency against IGFRK (compare **7** with **5**) and a similar loss against IRK. There were several possible explanations for this observation. The pyrrole NH group could have been making a favorable interaction with the active site that was removed by methylation. Alternatively, the methyl group may simply not fit into the binding site, or the methyl may adversely impact the bound conformation of the inhibitor. Reduction of the aldehyde moiety in **1** to give alcohol **3** resulted in an inactive compound, as did replacement of the ethyl ester groups with *N*,*N*-diethylamides (see **4** in Table 1). The inactivity of compound **4** could be attributed to steric factors. Molecular modeling studies revealed that, in low-energy conformations, the diethylamide groups in **4** were orthogonal to the plane of the pyrrole ring, in contrast to the almost coplanar geometry of the ethyl esters and the pyrrole ring in **1**, and it seemed possible that this difference could disrupt binding of **4** to the enzyme active site. The lack of potency of compound **3** indicated that the aldehyde group was required for activity, and it was hypothesized that this group might be involved in a reversible, covalent interaction with an active site residue. If this putative interaction involved formation of an imine with an active site Lys side chain, reduction of the imine would lead to an irreversible adduct and an inactivated enzyme.

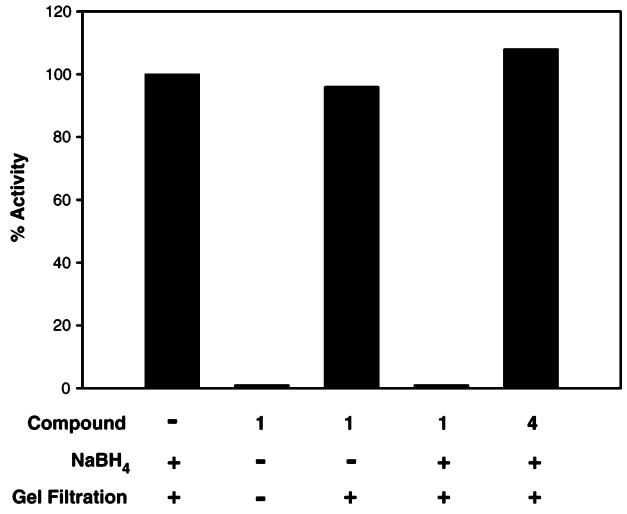

FIGURE 4: Irreversible inhibition of IGFRK activity following preincubation with compound **1** and $NaBH_4$. As detailed in the figure, the experiments were carried out in the absence of inhibitor or with compound **1** (100 μM) or **4** (100 μM), in the presence or absence of $NaBH_4$, and with or without gel filtration prior to determination of residual enzyme activity, shown as a percentage of control.

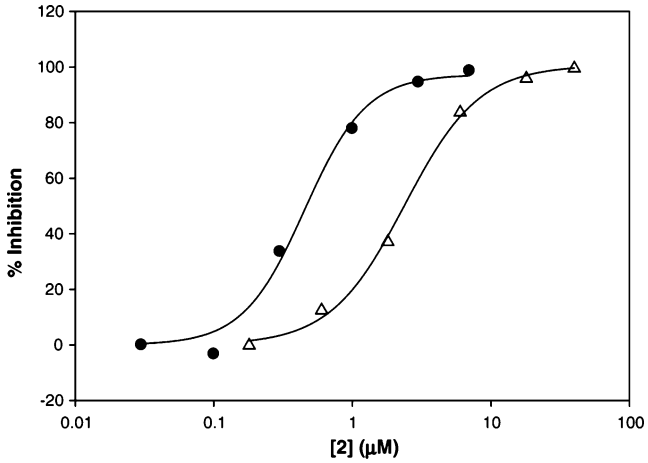

FIGURE 5: Irreversible inhibition of IGFRK (●) and IRK (△) activity following preincubation with $NaBH_4$ and varying **2** concentrations. Residual enzyme activity was determined following gel filtration. For compound **2**, IGFRK $IC_{50} = 0.45\ \mu M$ and IRK $IC_{50} = 2.4\ \mu M$.

$NaBH_4$ Reduction Generates an Irreversible Enzyme−Inhibitor Complex. To test the possibility that the aldehyde moiety of the active pyrrole compounds was forming a Schiff base with a lysine residue near the active site, a methodology for performing a mild reduction on an enzyme−inhibitor complex was devised. GST−IGFRK was preincubated with 100 μM compound **1** followed by $NaBH_4$ addition. After the reduction, unbound inhibitor and $NaBH_4$ were removed by gel filtration and the eluted enzyme was assayed for activity in the HTRF kinase assay. As shown in Figure 4, only reduction in the presence of compound **1** resulted in irreversible inhibition of kinase activity. In the absence of the compound or $NaBH_4$, all enzyme activity was recovered following gel filtration. In contrast, incubation with $NaBH_4$ and compound **4**, which was not an IGFRK inhibitor (Table 1) but did contain a free aldehyde, did not result in irreversible kinase inhibition. This observation indicated that the irreversible enzyme inhibition was not due to general

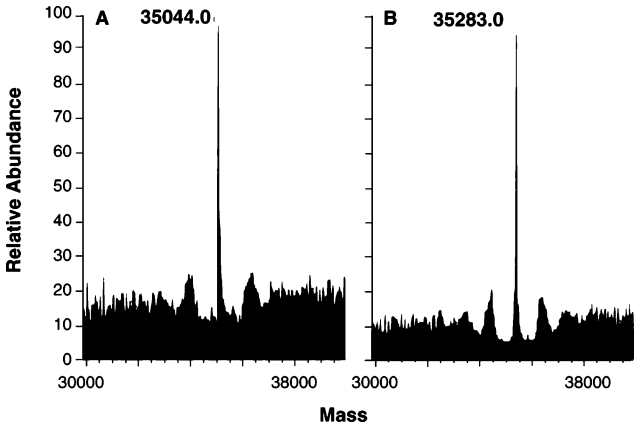

FIGURE 6: (A) Mass spectrum of the IGFRK306 fragment. (B) Mass spectrum of the IGFRK306 fragment following covalent modification with compound **1** and $NaBH_4$.

nonspecific modifications with reactive amino groups, but rather required binding of the inhibitor within the ATP binding pocket. To demonstrate that irreversible inhibition correlated with compound binding affinities, compound **2** was titrated in the $NaBH_4$ reaction using both GST−IGFRK and GST−IRK (Figure 5). It was found that **2** titrated to irreversibly inhibit both enzymes with IC_{50} values which are close to those determined in the enzyme autophosphorylation assay.[3] The ratio of IC_{50} values for irreversible inhibition by compound **2** (IGFRK $IC_{50} = 0.45$ μM; IRK $IC_{50} = 2.4$ μM; IRK:IGFRK ratio = 5) was also similar to that seen for the enzyme autophosphorylation assay (Table 3), further confirming the modest selectivity of compound **2** for the unactivated IGFRK enzyme.

Analysis of the Covalently Modified IGFRK Fragment. The observed mass of untreated IGFRK306 was 35 044 Da (LC−MS), in good agreement with the expected mass of 35 046 Da (Figure 6). Incubation of IGFRK306 with **1** and $NaBH_4$ resulted in a mass increase of 239 Da, consistent with the expected increase of 237 Da that would result from the incorporation of one molecule of inhibitor per enzyme molecule. The modified and control proteins were denatured and digested with trypsin, and 10 μg aliquots were analyzed by reverse-phase HPLC. Detection by UV absorbance at 220 or 280 nm indicated the presence of one major peak in the digest from the modified protein that was absent from the control (Figure 7A). Modified protein digest (50 μg) was chromatographed on the same column, and this peak was collected for further analysis. LC−MS indicated the presence of one peptide having a mass of 1627 Da (Figure 7B). If reaction with **1** did occur as predicted at a lysine residue, then trypsin cleavage at that amino acid would likely be prevented by the modification. Thus, the masses of two adjacent smaller tryptic peptides would be expected to account for the mass of the resulting peptide in addition to 237 Da contributed by the adduct. The equivalent unmodified peptide would therefore have a mass of 1390 Da. An examination of all tryptic peptides containing one missed cleavage site indicated that only one had the predicted mass, corresponding to residues 1000−1012 with the sequence ^{1000}-VAIKTVNEAASMR^{1012}. The identity of the isolated peptide was confirmed by automated sequence analysis. In addition, on the fourth cycle of the sequencing run, it was not possible to identify an amino acid, a result consistent with derivatization of the lysine at this position (data not shown). These results proved that aldehyde **1** had formed an adduct with residue Lys1003, which is conserved in the nucleotide binding site. It is interesting to note that compound **1** did not inhibit all enzymes with this conserved residue (see Table 2), although the possibility of Schiff base formation with lysines in other proteins cannot be excluded.

*Crystal Structure of IRK with Covalently Bound Compound **5**.* The IR kinase domain was treated with compound **5** and $NaBH_4$ (vide supra) to give the covalent IRK−**5** complex. This complex was crystallized and the structure determined in analogy with work by Hubbard et al. (*52*). The overall protein structure of the IR kinase domain (Figure 8) was essentially the same as the published structure (*52*). As expected, Lys1030 in the IRK active site (which corresponds to Lys1003 in IGFRK) had been modified by reductive alkylation with aldehyde **5**.

It was clear that formation of a covalent adduct between the active site lysine and the aldehyde moiety in these inhibitors was a critical determinant of potency, but the crystal structure of the covalently modified IRK domain revealed details of other key interactions between covalently bound **5** and the enzyme (see Figure 9). The pyrrole NH group formed a hydrogen bond with the main chain carbonyl of Asp1150 (shown in red). The *tert*-butyl group was bound in a hydrophobic pocket and interacted with the side chains of a number of residues, the most important being Phe1054, Leu1123, Phe1128, and Ile1148 (the hydrophobic residues mentioned are colored blue in Figure 9). The ethyl ester also made a number of interactions with lipophilic side chains, including Phe1007, Phe1044, and Val1074. The main interaction between the protein and the 3-ethyl substituent of the pyrrole was with the Met1051 side chain. Thus, the aldehyde group served to anchor the pyrrole inhibitor in the active site, the NH group engaged in hydrogen bonding, and the other ring substituents were involved in hydrophobic interactions.

The structural information explained some of the structure−activity data for these inhibitors (vide supra). For example, methylation of the pyrrole nitrogen deprived the molecule of a key hydrogen bonding interaction with the enzyme, resulting in a significant loss in potency (see Table 1). Additionally, the *tert*-butyl ester and the ethyl substituent on the pyrrole interacted primarily with hydrophobic sites on the enzyme, as hypothesized. The inactivity of the diethyl amide analogue **4** apparently resulted from the disruption caused by twisting the 4-position amide with respect to the pyrrole ring, consistent with expectations. In a modeling experiment, compound **4** was docked into the active site and subjected to energy minimization, which led the pyrrole ring to twist significantly in the active site, disrupting key interactions such as the hydrogen bond to the pyrrole NH group. Overall, the crystal structure clarified the observed data and may be useful in the design of more potent inhibitors of IGFRK.

The crystal structure did not provide a clear explanation for the observed selectivity of these compounds for IGFRK

[3] The IC_{50} values from the $NaBH_4$ inhibitor titration and the autophosphorylation titrations are roughly comparable despite there being no ATP present during the $NaBH_4$ reaction, because the autophosphorylation reaction was carried out at [ATP] $\approx K_m$. Thus, lowering [ATP] to zero will shift the IC_{50} by no more than 2-fold.

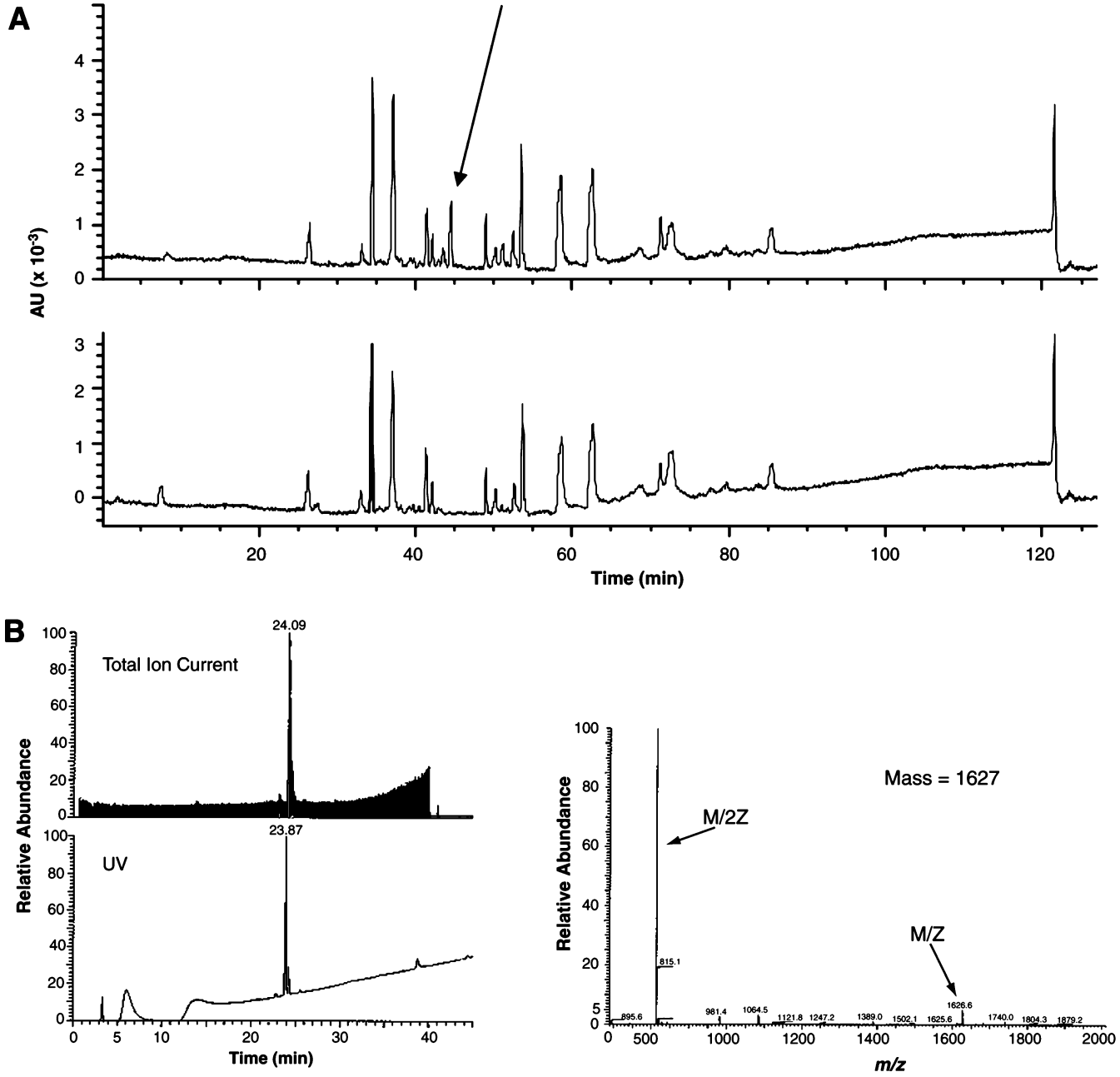

FIGURE 7: (A) Reverse-phase HPLC traces of tryptic digests of the IGFRK306 control (bottom trace) and IGFRK306 covalently modified by compound **1** (top trace). The arrow indicates the major new peak present in the digest of the enzyme following treatment with $NaBH_4$ and compound **1**. (B) LC−MS analysis of the new peak shown in panel A. The peak corresponded to a single peptide with a mass of 1627 Da.

over IRK. All of the IRK residues that were seen to interact with the inhibitor are conserved in IGFRK. Additionally, modeling studies on the covalent complex of **5** with IGFRK suggested that this complex was similar to the IRK−**5** crystal structure. In this analysis, compound **5** was docked as a Schiff base with Lys1003 in the active site of a homology model of IGFRK and the active site was subjected to energy minimization. The resulting modeled IGFRK−**5** complex (data not shown) was very similar to the crystal structure shown in Figures 8 and 9, with no substantial changes in the conformations of either inhibitor or active site side chains and no obvious differences in terms of enzyme−inhibitor interactions. It should be noted that the difference in inhibitory potency seen with the two enzymes was modest. The small differences in binding energy may be due to subtle alterations of the overall protein architecture between the two active sites. X-ray crystal structures of the unactivated apoenzymes IRK and IGFRK have revealed some differences in the ATP-binding pocket, notably in the activation loop and nucleotide-binding loop (*48*). While these nonliganded structures are not identical to the IRK−**5** complex, they demonstrate the possibility of conformational differences in the binding sites of IRK and IGFRK. Relatively small changes in the interactions between the protein and inhibitor could produce the observed differences in IC_{50} values, and such minor effects may be difficult to detect by these structural and calculational approaches.

CONCLUSION

A novel class of pyrrole-based IGFRK inhibitors has been discovered. The compounds exhibited modest selectivity against the closely related IRK, and they preferentially

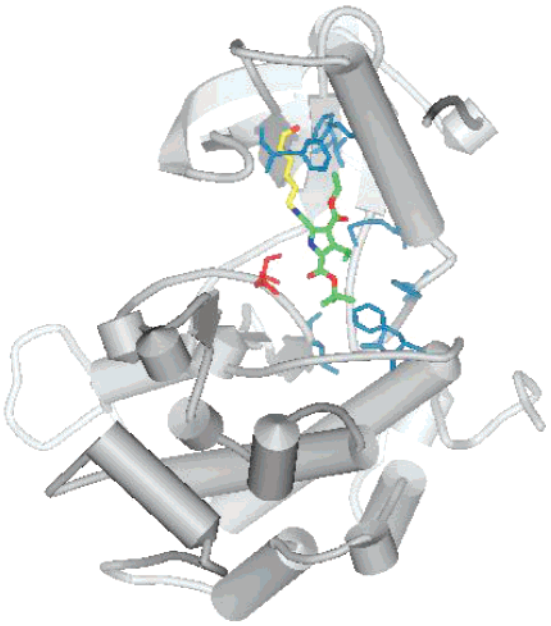

FIGURE 8: X-ray crystal structure of the IRK domain covalently modified by compound **5**. The modified Lys1030 is colored yellow, and the carbon atoms of the pyrrole inhibitor are colored green. Asp1150 is colored red, and residues that make key hydrophobic contacts with the inhibitor are colored blue.

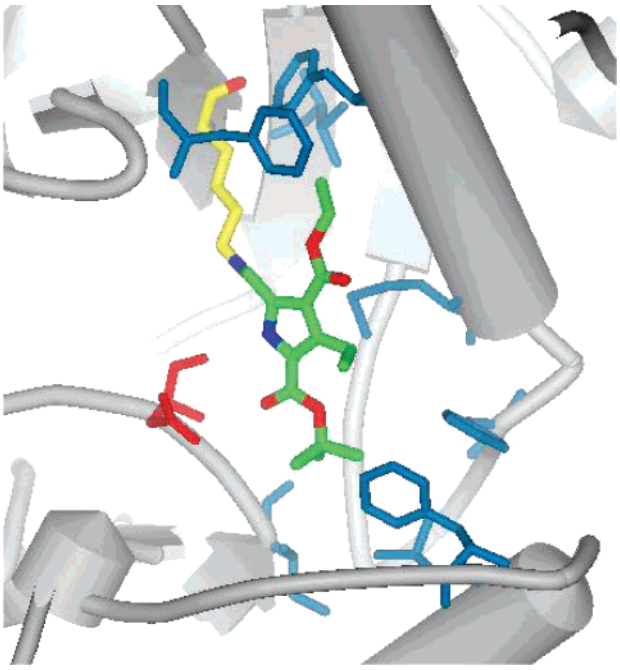

FIGURE 9: Close-up of the active site of the covalent IRK−**5** complex. The color scheme is identical to that in Figure 8.

inhibited the unactivated forms of both kinases. The selectivity for IGFRK versus IRK was observed in several in vitro enzyme inhibition assays and also in a whole cell assay. These inhibitors contained a key aldehyde functionality which apparently formed a Schiff base with the IGFRK active site residue Lys1003, and this covalent complex could be trapped by borohydride reduction. A crystal structure of the covalently modified IRK domain revealed the key interactions between the inhibitor and the active site. This information may facilitate the development of clinically useful inhibitors of IGF-1R.

ACKNOWLEDGMENT

We thank Keith Rickert for helpful discussions and Jill Williams for preparation of figures.

REFERENCES

1. Hanahan, D., and Weinberg, R. A. (2000) The hallmarks of cancer, *Cell 100*, 57−70.
2. Blume Jensen, P., and Hunter, T. (2001) Oncogenic kinase signalling, *Nature 411*, 355−365.
3. Gschwind, A., Fischer, O. M., and Ullrich, A. (2004) The discovery of receptor tyrosine kinases: Targets for cancer therapy, *Nat. Rev. Cancer 4*, 361−370.
4. Vogel, C. L., Cobleigh, M. A., Tripathy, D., Gutheil, J. C., Harris, L. N., Fehrenbacher, L., Slamon, D. J., Murphy, M., Novotny, W. F., Burchmore, M., Shak, S., Stewart, S. J., and Press, M. (2002) Efficacy and safety of trastuzumab as a single agent in first-line treatment of HER2-overexpressing metastatic breast cancer, *J. Clin. Oncol. 20*, 719−726.
5. Blackledge, G., and Averbuch, S. (2004) Gefitinib ('Iressa', ZD1839) and new epidermal growth factor receptor inhibitors, *Br. J. Cancer 90*, 566−572.
6. Werner, H., and LeRoith, D. (1996) The role of the insulin-like growth factor system in human cancer, *Adv. Cancer Res. 68*, 183−223.
7. Wang, Y., and Sun, Y. (2002) Insulin-like growth factor receptor-1 as an anti-cancer target: Blocking transformation and inducing apoptosis, *Curr. Cancer Drug Targets 2*, 191−207.
8. Baserga, R., Peruzzi, F., and Reiss, K. (2003) The IGF-1 receptor in cancer biology, *Int. J. Cancer 107*, 873−877.
9. LeRoith, D., Werner, H., BeitnerJohnson, D., and Roberts, C. T. (1995) Molecular and cellular aspects of the insulin-like growth factor I receptor, *Endocr. Rev. 16*, 143−163.
10. O'Connor, R., Kauffmann Zeh, A., Liu, Y., Lehar, S., Evan, G. I., Baserga, R., and Blattler, W. A. (1997) Identification of domains of the insulin-like growth factor I receptor that are required for protection from apoptosis, *Mol. Cell. Biol. 17*, 427−435.
11. Chen, H., Yan, G. C., and Gishizky, M. L. (1998) Identification of structural characteristics that contribute to a difference in antiapoptotic function between human insulin and insulin-like growth factor I receptors, *Cell Growth Differ. 9*, 939−947.
12. Resnicoff, M., Abraham, D., Yutanawiboonchai, W., Rotman, H. L., Kajstura, J., Rubin, R., Zoltick, P., and Baserga, R. (1995) The insulin-like growth factor I receptor protects tumor cells from apoptosis in vivo, *Cancer Res. 55*, 2463−2469.
13. Sell, C., Baserga, R., and Rubin, R. (1995) Insulin-like growth factor I (IGF-I) and the IGF-I receptor prevent etoposide-induced apoptosis, *Cancer Res. 55*, 303−306.
14. D'Ambrosio, C., Valentinis, B., Prisco, M., Reiss, K., Rubini, M., and Baserga, R. (1997) Protective effect of the insulin-like growth factor I receptor on apoptosis induced by okadaic acid, *Cancer Res. 57*, 3264−3271.
15. Zhang, L. (1997) Gene expression profiles in normal and cancer cells, *Science 276*, 1268−1272.
16. Cullen, K. J., Yee, D., Sly, W. S., Perdue, J., Hampton, B., Lippman, M. E., and Rosen, N. (1990) Insulin-like growth factor receptor expression and function in human breast cancer, *Cancer Res. 50*, 48−53.
17. Guo, Y. S., Narayan, S., Yallampalli, C., and Singh, P. (1992) Characterization of insulinlike growth factor I receptors in human colon cancer, *Gastroenterology 102*, 1101−1108.
18. Tricoli, J. V., Rall, L. B., Karakousis, C. P., Herrera, L., Petrelli, N. J., Bell, G. I., and Shows, T. B. (1986) Enhanced levels of insulin-like growth factor messenger RNA in human colon carcinomas and liposarcomas, *Cancer Res. 46*, 6169−6173.
19. Ellis, M. J., Jenkins, S., Hanfelt, J., Redington, M. E., Taylor, M., Leek, R., Siddle, K., and Harris, A. (1998) Insulin-like growth factors in human breast cancer, *Breast Cancer Res. Treat. 52*, 175−184.
20. Stattin, P., Rinaldi, S., Biessy, C., Stenman, U. H., Hallmans, G., and Kaaks, R. (2004) High levels of circulating insulin-like growth factor-I increase prostate cancer risk: A prospective study in a population-based nonscreened cohort, *J. Clin. Oncol. 22*, 3104−3112.
21. Ma, J., Pollak, M. N., Giovannucci, E., Chan, J. M., Tao, Y., Hennekens, C. H., and Stampfer, M. J. (1999) Prospective study

of colorectal cancer risk in men and plasma levels of insulin-like growth factor (IGF)-I and IGF-binding protein-3, *J. Natl. Cancer Inst. 91*, 620−625.
22. Manousos, O., Souglakos, J., Bosetti, C., Tzonou, A., Chatzidakis, V., Trichopoulos, D., Adami, H. O., and Mantzoros, C. (1999) IGF-I and IGF-II in relation to colorectal cancer, *Int. J. Cancer 83*, 15−17.
23. Hankinson, S. E., Willett, W. C., Colditz, G. A., Hunter, D. J., Michaud, D. S., Deroo, B., Rosner, B., Speizer, F. E., and Pollak, M. (1998) Circulating concentrations of insulin-like growth factor-I and risk of breast cancer, *Lancet 351*, 1393−1396.
24. Hakam, A., Yeatman, T. J., Lu, L., Mora, L., Marcet, G., Nicosia, S. V., Karl, R. C., and Coppola, D. (1999) Expression of insulin-like growth factor-1 receptor in human colorectal cancer, *Hum. Pathol. 30*, 1128−1133.
25. Kawamoto, K., Onodera, H., Kondo, S., Kan, S., Ikeuchi, D., Maetani, S., and Imamura, M. (1998) Expression of insulin-like growth factor-2 can predict the prognosis of human colorectal cancer patients: Correlation with tumor progression, proliferative activity and survival, *Oncology 55*, 242−248.
26. Turner, B. C., Haffty, B. G., Narayanan, L., Yuan, J., Havre, P. A., Gumbs, A. A., Kaplan, L., Burgaud, J. L., Carter, D., Baserga, R., and Glazer, P. M. (1997) Insulin-like growth factor-I receptor overexpression mediates cellular radioresistance and local breast cancer recurrence after lumpectomy and radiation, *Cancer Res. 57*, 3079−3083.
27. Sepp Lorenzino, L. (1998) Structure and function of the insulin-like growth factor I receptor, *Breast Cancer Res. Treat. 47*, 235−253.
28. Ablooglu, A. J., and Kohanski, R. A. (2001) Activation of the insulin receptor's kinase domain changes the rate-determining step of substrate phosphorylation, *Biochemistry 40*, 504−513.
29. Kulik, G., Klippel, A., and Weber, M. J. (1997) Antiapoptotic signalling by the insulin-like growth factor I receptor, phosphatidylinositol 3-kinase, and Akt, *Mol. Cell. Biol. 17*, 1595−1606.
30. Dudek, H., Datta, S. R., Franke, T. F., Birnbaum, M. J., Yao, R., Cooper, G. M., Segal, R. A., Kaplan, D. R., and Greenberg, M. E. (1997) Regulation of neuronal survival by the serine-threonine protein kinase Akt, *Science 275*, 661−665.
31. Dews, M., Prisco, M., Peruzzi, F., Romano, G., Morrione, A., and Baserga, R. (2000) Domains of the insulin-like growth factor I receptor required for the activation of extracellular signal-regulated kinases, *Endocrinology 141*, 1289−1300.
32. Kalebic, T., Blakesley, V., Slade, C., Plasschaert, S., Leroith, D., and Helman, L. J. (1998) Expression of a kinase-deficient IGF-I-R suppresses tumorigenicity of rhabdomyosarcoma cells constitutively expressing a wild-type IGF-I-R, *Int. J. Cancer 76*, 223−227.
33. Kato, H., Faria, T. N., Stannard, B., Roberts, C. T., and Leroith, D. (1994) Essential Role of Tyrosine Residues 1131, 1135, and of 1136 of the Insulin-Like Growth Factor-I (Igf-I) Receptor in Igf-I Action, *Mol. Endocrinol. 8*, 40−50.
34. Hongo, A., D'Ambrosio, C., Miura, M., Morrione, A., and Baserga, R. (1996) Mutational analysis of the mitogenic and transforming activities of the insulin-like growth factor I receptor, *Oncogene 12*, 1231−1238.
35. Garcia Echeverria, C., Pearson, M. A., Marti, A., Meyer, T., Mestan, J., Zimmermann, J., Gao, J., Brueggen, J., Capraro, H. G., Cozens, R., Evans, D. B., Fabbro, D., Furet, P., Porta, D. G., Liebetanz, J., Martiny Baron, G., Ruetz, S., and Hofmann, F. (2004) In vivo antitumor activity of NVP-AEW541-A novel, potent, and selective inhibitor of the IGF-IR kinase, *Cancer Cell 5*, 231−239.
36. Mitsiades, C. S., Mitsiades, N. S., McMullan, C. J., Poulaki, V., Shringarpure, R., Akiyama, M., Hideshima, T., Chauhan, D., Joseph, M., Libermann, T. A., Garcia Echeverria, C., Pearson, M. A., Hofmann, F., Anderson, K. C., and Kung, A. L. (2004) Inhibition of the insulin-like growth factor receptor-1 tyrosine kinase activity as a therapeutic strategy for multiple myeloma, other hematologic malignancies, and solid tumors, *Cancer Cell 5*, 221−230.
37. Burtrum, D., Zhu, Z. P., Lu, D., Anderson, D. M., Prewett, M., Pereira, D. S., Bassi, R., Abdullah, R., Hooper, A. T., Koo, H., Jimenez, X., Johnson, D., Apblett, R., Kussie, P., Bohlen, P., Witte, L., Hicklin, D. J., and Ludwig, D. L. (2003) A fully human monoclonal antibody to the insulin-like growth factor I receptor blocks ligand-dependent signaling and inhibits human tumor growth in vivo, *Cancer Res. 63*, 8912−8921.
38. Ullrich, A., Gray, A., Tam, A., Tang-Feng, T., Tsubokawa, M., and Collins, C. (1986) Insulin-like growth factor 1 receptor primary structure: Comparison with the insulin receptor suggests structural determinants that define functional specificity, *EMBO J. 5*, 2503−2512.
39. Thyrann, T., and Lightner, D. A. (1995) Oxidation of Pyrrole-Methyl to Formyl with Ceric Ammonium Nitrate, *Tetrahedron Lett. 36*, 4345−4348.
40. Grigg, R., Johnson, A. W., and Wasley, J. W. F. (1963) 2,2′-Bipyrroles, *J. Chem. Soc. 30*, 359−366.
41. Brittain, J. M., Jones, A. R., Jones, R. O., and King, T. J. (1981) Pyrrole Studies. Part 26. A Novel Thermochromic and Photochromic Pyrrole System, *J. Chem. Soc., Perkin Trans. 1*, 2656−2661.
42. Welch, S. C., Assercq, J.-M., Loh, J.-P., and Glase, S. A. (1987) 3-Chloro-2-[(diethoxyphosphoryl)oxy]-1-propene: A New Reagent for a "One-Pot" Cyclopentenone Annelation. Syntheses of Desoxyallethrolone, cis-Jasmone, and Methylenomycin B, *J. Org. Chem. 52*, 1440−1450.
43. Mohamadi, F., Richards, N. G. J., Guida, W. C., Liskamp, R., Lipton, M., Caufield, C., Chang, G., Hendrickson, T., and Still, W. C. (1990) Macromodel: An integrated software system for modeling organic and bioorganic molecules using molecular mechanics, *J. Comput. Chem. 11*, 440−467.
44. Ullrich, A., Bell, J. R., Chen, E. Y., Herrera, R., Petruzzelli, L. M., Dull, T. J., Gray, A., Coussens, L., Liao, Y. C., Tsubokawa, M., et al. (1985) Human insulin receptor and its relationship to the tyrosine kinase family of oncogenes, *Nature 313*, 756−761.
45. Park, Y. W., Cummings, R. T., Wu, L., Zheng, S., Cameron, P. M., Woods, A., Zaller, D. M., Marcy, A. I., and Hermes, J. D. (1999) Homogeneous proximity tyrosine kinase assays: Scintillation proximity assay versus homogeneous time-resolved fluorescence, *Anal. Biochem. 269*, 94−104.
46. Kendall, R. L., Rutledge, R. Z., Mao, X., Tebben, A. J., Hungate, R. W., and Thomas, K. A. (1999) Vascular Endothelial Growth Factor Receptor KDR Tyrosine Kinase Activity Is Increased by Autophosphorylation of Two Activation Loop Tyrosine Residues, *J. Biol. Chem. 274*, 6453−6460.
47. Clauser, K. R., Baker, P., and Burlingame, A. L. (1999) Role of accurate mass measurement (±10 ppm) in protein identification strategies employing MS or MS/MS and database searching, *Anal. Chem. 71*, 2871−2882.
48. Munshi, S., Kornienko, M., Hall, D. L., Reid, J. C., Waxman, L., Stirdivant, S. M., Darke, P. L., and Kuo, L. C. (2002) Crystal structure of the Apo, unactivated insulin-like growth factor-1 receptor kinase: Implication for inhibitor specificity, *J. Biol. Chem. 277*, 38797−38802.
49. Otwinowski, Z., and Minor, W. (1997) Processing of X-ray diffraction data collected in oscillation mode, *Methods Enzymol. 276*, 307−326.
50. Navaza, J. (1994) Amore: An Automated Package for Molecular Replacement, *Acta Crystallogr. A50*, 157−163.
51. Bailey, S. (1994) The Ccp4 Suite: Programs for Protein Crystallography, *Acta Crystallogr. D50*, 760−763.
52. Hubbard, S. R., Wei, L., Ellis, L., and Hendrickson, W. A. (1994) Crystal structure of the tyrosine kinase domain of the human insulin receptor, *Nature 372*, 746−754.
53. Brunger, A. T., Adams, P. D., Clore, G. M., DeLano, W. L., Gros, P., Grosse Kunstleve, R. W., Jiang, J. S., Kuszewski, J., Nilges, M., Pannu, N. S., Read, R. J., Rice, L. M., Simonson, T., and Warren, G. L. (1998) Crystallography & NMR system: A new software suite for macromolecular structure determination, *Acta Crystallogr. D54*, 905−921.

BI0500628